Cause for quasi-biweekly oscillation of zonal location of western Pacific subtropical high during boreal summer

Shuangyan Yang, Tim Li

PII: S0169-8095(20)30019-3

DOI: https://doi.org/10.1016/j.atmosres.2020.105079

Reference: ATMOS 105079

To appear in: *Atmospheric Research*

Received date: 6 January 2020

Revised date: 4 May 2020

Accepted date: 1 June 2020

Please cite this article as: S. Yang and T. Li, Cause for quasi-biweekly oscillation of zonal location of western Pacific subtropical high during boreal summer, *Atmospheric Research* (2019), https://doi.org/10.1016/j.atmosres.2020.105079

Cause for Quasi-Biweekly Oscillation of Zonal Location of Western Pacific Subtropical High during Boreal Summer

Shuangyan Yang[1], Tim Li[1, 2]

[1] Key Laboratory of Meteorological Disaster, Ministry of Education (KLME)/Joint International Research Laboratory of Climate and Environmental Change (ILCEC)/Collaborative Innovation Center on Forecast and Evaluation of Meteorological Disasters (CIC-FEMD), Nanjing University of Information Science and Technology, Nanjing, China

[2] International Pacific Research Center and Department of Atmospheric Sciences, University of Hawaii at Manoa, Honolulu, Hawaii

Submitted to Atmospheric Research on January 6, 2020

Revised on May 4, 2020

Corresponding author: Tim Li, International Pacific Research Center and Department of Atmospheric Sciences, University of Hawaii at Manoa, Honolulu, Hawaii 96822.

Email: timli@hawaii.edu. Phone: (808) 956-9427. Fax: (808) 956-9425

ABSTRACT

The cause for zonal oscillation of the western Pacific subtropical high (WPSH) on a quasi-biweekly (10–20-day) timescale was investigated. Both relative vorticity and geopotential height anomalies exhibit a maximum activity center over the western edge of the climatological WPSH. The quasi-biweekly WPSH oscillation is closely related to a northwestward-propagating quasi-biweekly oscillation (QBWO) mode over the western North Pacific (WNP). A real-time index of the WNP-QBWO is used to analyze the influence of the northwestward-propagating WNP-QBWO mode on the zonal shift of the WPSH. The QBWO convection anomaly propagates northwestward from the tropical WNP to East Asia. It is the alternation of a positive and a negative geopotential height anomaly during the northwestward propagating journey that leads to the zonal oscillation of the WPSH. Once a positive (negative) QBWO geopotential height propagates from tropical WNP into the western edge of the climatological WPSH, it leads to a western extension (eastern retreat) of the WPSH. This provides a monitoring and predicting method of the zonal shift of the WPSH at an extended rang by using the real-time index. Two mechanisms are likely responsible for the northwestward propagation of the WNP-QBWO mode. The first is internal atmospheric dynamics. Both positive vorticity and moisture anomalies appear to the northwest of the QBWO convection, favoring the northwestward propagation. The second is attributed to the atmosphere-ocean interaction. A warm sea surface temperature (SST) anomaly leads the QBWO convection by an approximately 90-degree phase, and both the SST and convection anomalies move northwestward.

Keywords: zonal oscillation of the WPSH, QBWO over the WNP, real-time index

1. Introduction

The western Pacific subtropical high (WPSH) is one major component of East Asian summer monsoon system (Lau and Li, 1984; Wang and Chen, 2012). As a permanent circulation system at the northern hemisphere, the WPSH is of great importance in tropical cyclone activities (both their genesis and moving tracks) over the western North Pacific (Ho et al., 2004; Wang et al., 2013) and precipitation/temperature over East Asia (Lau and Weng, 2002; Matsumura et al., 2015).

One of the most dominant features of the WPSH is its zonal oscillation on the intra-seasonal timescale (Ren et al., 2013), which has comparable importance as that on the interannual (Sui et al., 2007; Wu and Zhou, 2008) and interdecadal (Gong and Ho, 2002; Huang et al., 2015) timescales.

The zonal oscillation of the WPSH on the intraseasonal timescale evidently influences the sub-seasonal East Asian rainfall by regulating the transport of the vapor from ocean to land (Liu et al., 2008). Mao et al. (2010) revealed that the 20–50-day oscillation of summer Yangtze rainfall is due to the intraseasonal variations of the WPSH. The eastward retreat of the WPSH is responsible for the dry condition in the Yangtze Basin, while the westward extension results in the wet condition over the region. Yang et al. (2010) found that the 21–30-day mode of summer rainfall over the lower reach of the Yangtze River basin is mainly related to the westward extension of the WPSH. Ren et al. (2013) reported that the positive/negative sub-seasonal rainfall anomaly over the middle and lower reaches of the Yangtze River valley during early

and late summer is accompanied by the westward/eastward movement of the WPSH western edge. The intraseasonal zonal movement of the WPSH coordinates with other circulation system, such as the South Asian High (SAH) which also shows an intraseasonal zonal shift revealed by previous studies (e.g., Ren et al., 2015; Yang and Li, 2016). The intraseasonal zonal movement of the WPSH and the SAH goes in opposite directions (Jia and Yang, 2013; Ren et al., 2015; Guan et al., 2018), that is, when the WPSH extends westward, the SAH stretches eastward; when the WPSH retreats eastward, the SAH moves westward. The coupled zonal motion of the WPSH and the SAH on the intraseasonal timescale contributes to the rainfall anomalies over East China (Chen and Zhai, 2016).

The atmospheric quasi-biweekly oscillation (QBWO) is one of the most prevailing modes at northern hemisphere on the intraseasonal timescale (Wen et al., 2011; Yang and Li, 2017a, b). Although the QBWO of the WPSH along longitude was mentioned in previous papers, its detail evolution process and its relationship to the QBWO mode needs further investigation. Since the QBWO of the WPSH zonal shift plays an important role in the regional sub-seasonal variation, finding an effective prediction method to predict the quasi-biweekly evolution of the WPSH zonal location may improve the extended range forecast which is the most challenging issue facing the weather and climate community.

The first objective of this study is to document the structure and evolution features of the QBWO of the WPSH zonal shift and the associated lower- and mid-tropospheric circulation anomaly in detail. The second purpose is to probe into a

cause for the QBWO of the zonal oscillation of the WPSH, through analyze the relationship between the QBWO of the WPSH zonal shift and a real-time index for monitoring of the QBWO over the tropical WNP.

The remaining part of this paper is organized as follows. Data and methodology used in this study are described in Sect. 2. The structure and evolution characteristics of the zonal QBWO of the WPSH during boreal summer are displayed in Sect. 3. In Sect. 4, the possible cause of the zonal QBWO of the WPSH is proposed, in which the northwestward-propagating QBWO mode over the WNP plays a crucial role. At the end of this section, the possible mechanisms of the northwestward propagation of the WNP-QBWO are discussed. Conclusions and discussions are given in Sect. 5.

2. Data and methodology

The National Centers for Environmental Prediction-Department of Energy (NCEP-DOE) reanalysis data (Kanamitsu et al., 2002) at a horizontal resolution of 2.5°×2.5° for the period 1979–2014 is used in this study, including daily zonal wind u, meridional wind v, geopotential height Z. Relative vorticity ζ is calculated using u and v. The vertically integrated apparent heat source $\langle Q_1 \rangle$ is calculated according to Yanai et al. (1973). Daily mean outgoing longwave radiation (OLR) at a 2.5°×2.5° grid for 1979–2013 from the National Oceanic and Atmospheric Administration (NOAA) (Liebmann and Smith, 1996) is also used as a proxy for convection. The variables at a 1.5° × 1.5° horizontal resolution also used in a meridional-vertical profile in Fig. 10 is derived from the European Centre for Medium-Range Weather

Forecasts (ECMWF) Interim reanalysis (ERA-Interim; Dee et al., 2011). In addition, a new real-time index for the QBWO over the WNP is used in this study, which proposed by Qian et al. (2019).

In this study, the quasi-biweekly signal was obtained by a Lanczos bandpass filter (Duchon, 1979). Prior to the filtering, the mean and first four harmonics of the annual cycle were removed from each field to remove the slow annual cycle, but keep the climatological intraseasonal oscillation. Summer time is defined as the period of Jun–July–August (JJA). In addition, the phase propagation vector and temporal coherence of the vorticity anomaly are calculated based on one-point correlation maps (Lau and Lau, 1990). For a given grid, the vorticity anomaly at this grid point is regarded as a reference time series. A lead-lag correlation is calculated between the time series at the base point and the time series at each surrounding grid points, from lagged day –5 to day +5. The direction of the phase propagation vector at a base-point is estimated from the orientation of the line segment pointing from the strongest positive correlation center at day –5 to that at day +5. The propagation velocity is calculated by dividing the distance of the line segment by the time interval (i.e., 10 days). The temporal coherence at a base-point is defined as the average of the strongest positive lagged correlation coefficient at day –5 and the strongest one at day +5.

3. Temporal-spatial evolution of zonal oscillation of the WPSH

3.1 Dominant periodicity of the zonal oscillation

Figure 1 shows the standard deviation (STD) of relative vorticity ζ (ζ_{850}, ζ_{500}) and geopotential height Z (Z_{850}, Z_{500}) anomalies at 850hPa and 500hPa. The shown STD has been normalized by its zonal mean value following Sui et al. (2007). Also shown in Fig. 1 are the climatological ζ and Z in shading to highlight the position of the climatological WPSH. For ζ_{850} and ζ_{500}, the surrounded area by isoline of -5×10^{-6} s^{-1} can be considered as the main body of the WPSH. For Z_{850} (Z_{500}), the surrounded area by isoline of 1500~1520 (5870~5880) gpm can be referred to as the main body of the WPSH. It is seen that a maximum STD center (box region of 20°–30°N, 120°–140°E) appears at the western edge of the climatological WPSH.

Referred to Wei et al. (2019), we use ζ rather than Z to define a WPSH index in order to reduce the increase trends of the WPSH that caused by the anthropogenic forcing. Since the WPSH is much more stable and stronger at lower troposphere than middle troposphere (Lu et al., 2008), the lower tropospheric ζ (i.e., ζ_{850}) is selected to define a relative vorticity index (RVI). The RVI is defined as the box-averaged ζ_{850} (i.e., box region in Fig. 1) to measure the zonal shift of the WPSH. Figure 2 plots the composite ζ_{850}, Z_{850} and Z_{500} during higher negative and higher positive RVI events. As shown by each composite field, a higher negative value suggests a western extension of the WPSH, while a higher positive one implies an eastern retreat of the WPSH. The composite ζ_{500} (figure omitted) shows a similar feature. These indicate that the defined RVI can well depict the zonal oscillation of the WPSH at both lower troposphere and middle troposphere.

Given that the RVI can well reflect the zonal displacement of the WPSH, the

dominant periodicity of the RVI could represent the cycle time of the zonal oscillation of the WPSH. Figure 3a displays the power spectral analysis of the RVI. It is shown that significant spectral peak of the RVI includes both intraseasonal and synoptic time scales, and the first leading spectral peak appears at ~18 days. In the following sections, we will focus on the intraseasonal oscillation of the WPSH zonal shift. The atmospheric intraseasonal oscillation generally refers to the atmospheric oscillation above 10 days, but within 100 days and contains two well concerned bands with 30–60-day period and 10–20-day period. Therefore, the period of 10–20 days is selected, which includes the leading spectral peak of ~18 days. Thus, our focus is the statistically significant periodicity at the band of 10–20 days, indicating a zonal QBWO of the WPSH. Figure 3b shows the STD of the ζ'_{850} (a prime denotes a 10–20-day filtered field, same as below). Again, the maximum activity center is located at the western edge of the climatological WPSH (box region), which is also found in Fig. 3c, the STD of non-filtered ζ_{850} anomaly. Unlike Fig. 1, what we show in Fig. 3b and Fig. 3c is the non-normalized STD, to intuitively display the ratio of the 10–20-day vorticity variability to the non-filtered vorticity variability. We defined a higher negative RVI$'$ (i.e., RVI$'$ < −1.0σ) as a westward extension event, while a higher positive RVI$'$ (i.e., RVI$'$ > +1.0σ) as an eastward withdrawal event. Total 110 eastward withdrawal events and 117 westward extension events are selected for composite analysis in this section.

3.2 Evolution of the zonal oscillation

Figure 4a shows the lagged composite Z'_{850} (shading) from day 0 to +6 with an interval of 2 days. Because the eastward withdrawal event composite is approximately a mirror image of the westward extension events for the filtered fields, the composite is obtained by averaging the difference between the eastward withdrawal events and westward extension events (the former minus the latter). Day 0 means the time when the maximum/minimum Z'_{850} appears at the key area. As shown in Fig. 4a, at day 0, a statistically significant negative height anomaly can be found over the key area of 20°–30°N, 120°–140°E, i.e., the western edge of the climatological WPSH. The height anomaly gradually changes with lag days. At day +6, the anomaly altered its sign in the key area, suggesting that the western edge of the climatological WPSH is controlled by a positive height anomaly. The alteration of the sign of the Z'_{850} reflects a zonal oscillation of the WPSH. To show the zonal shift clearly, we also plot the composite raw Z_{850} field during the eastward withdrawal events by contour in Fig. 4a, with the 1520-line in red. The red arrows connect the intersections of the ridge line and 1520-line, which depict a gradual western expansion of the WPSH vividly.

A similar evolution feature is also found in the Z'_{500}, Fig. 4a suggesting an equivalent barotropic vertical structure of the 10–20-day height anomaly. To reveal the zonal movement of the WPSH, the raw Z_{500} during eastward withdrawal events is also shown in Fig. 4b by solid contour, and the 5880-line is highlighted in blue. During the eastward withdrawal events, the 5880-line gradually retreats eastward from day −6 to 0 (figure omitted), and expands westward from day 0 to +6, since the height anomaly over the key area gradually changes. The intersections of the ridge

line and 5880-line are connected by blue arrow in Fig. 4b. It seems that the variation of the height anomaly at the western edge is related to the northwestward propagation of the tropical QBWO signal, which will be discussed in next section.

To clearly show the temporal-spatial evolution of the quasi-biweekly signals corresponding to the zonal shift of the WPSH, the composite maps of the ζ'_{850}, OLR′, and $<Q_1>'$ from day −6 to day 0, which approximates half a cycle, are displayed in Fig. 5. At day −6, a negative vorticity anomaly (shading) appears at both the tropical WNP and the key area of 20°–30°N, 120°–140°E, and simultaneously a positive anomaly is located between the two regions. This tripole structure tilted southeast-northwest shifts northwestward gradually. At day 0, the key area is governed by the preexisted positive anomaly since the northwestward propagation of the ζ'_{850}. At this day, the ζ'_{850} distribution is similar to Z'_{850} in Fig. 4a, but with an opposite sign, following well the quasi-geostrophic relationship. The OLR′ field (contour) also moves northwestward from day −6 to 0. At day −6, a negative OLR′ center is located at near (10°N, 155°E), and this negative center moves northwestward to (22.5°N, 132.5°E) at day 0. Generally, the $<Q_1>'$ maxima region corresponds well to the OLR′ minima, as shown in Fig. 5b, indicating that the low-latitude diabatic heating is dominated by the convection heating. Figures 4 and 5 clearly shown the connection of the zonal shift of the WPSH to the northwestward-propagating QBWO in the WNP, that is, a westward shift of the WPSH is associated with the arrival of suppressed phase of the QBWO, and vice versa.

4. Cause for the zonal oscillation of the WPSH

The above linkage between the WPSH and the QBWO was derived based on the WPSH index. To further demonstrate their connection, in this section we analyze their relationship based on the QBWO mode in the WNP. We firstly calculate the phase propagation vector and temporal coherence of the ζ'_{850}, to exhibit the propagating feature of the QBWO mode over the WNP. Temporal coherence indicates how well a migratory signal is maintained through its evolution in time. As shown in Fig. 6, the ζ'_{850} over the WNP region propagates northwestward, and almost all velocity vectors exceed a 0.05 significance level indicated by the temporal coherence in shading. The box area represents the key area at the western edge of the climatological related to the zonal shift of the WPSH. The propagation vector illustrates that the QBWO disturbance over the tropical WNP can propagate into the key area, further suggesting a possible influence of the tropical QBWO on the zonal shift of the WPSH.

Recently, Qian et al. (2019) proposed a new real-time index of the WNP-QBWO. Two steps are used to obtain this index. First, to derive the first two typical QBWO modes, an extended empirical orthogonal function (EEOF) analysis is conducted on the –4-, –2- and 0-day lags of bandpass-filtered OLR anomaly during summer time in the WNP region. Second, projecting the –4, –2 and 0 days of non-bandpass-filtered OLR anomaly onto the first two typical EEOF modes to obtain the WNP-QBWO index (i.e., WNP-QBWOI1 and WNP-QBWOI2). While the amplitudes of the WNP-QBWO (WNP-QBWOI) is defined as $(\text{WNP-QBWO1}^2 + \text{WNP-QBWO2}^2)^{1/2}$. According to the WNP-QBWOI1 and WNP-QBWOI2, each cycle has divided into eight phases. The eight phases represent different locations of the QBWO convection

center. The phase-space diagram is depicted in Fig. 7. The events of WNP-QBWOI <1.0 (center circle in Fig. 7) is considered as weak QBWO event in this study. To reveal the influence of the WNP-QBWO on the zonal oscillation of the WPSH, we analysis the evolution of the WPSH with the WNP-QBWO phase based on phase-composite method. In this study, we only use active WNP-QBWO events (i.e., WNP-QBWOI >1.0) during 1980–2012 for composite analysis. In each phase, the number of active events and their average amplitude is marked in Fig. 7. For example, there are 232 active events in phase 1 and their average amplitude is 1.77. Statistical results show that there is no marked difference in the amplitude and event number among each phase.

Figure 8 displays the composite ζ'_{850} (black contour) and OLR' (shading) from phase 1 to 8. Also shown is the mean 5880 isoline in each phase, representing the average location of the WPSH. As shown, from phase 4 to 8, a negative OLR' center moves northwestward from the WNP, crossing Philippine sea, to the South China Sea (SCS), and from phase 1 to 3, the negative center continue to propagate northwestward from the SCS to East Asia. Since the associated vorticity anomaly propagates northwestward into the key area, 5880 isoline shows an eastern-western movement, i.e., a zonal oscillation of the WPSH. Gradually, the area-mean ζ'_{850} over the key area (20°–30°N, 120°–140°E) decreases from phase 1 to 5. Simultaneously, the mean Z'_{850} over this key area increases gradually, leading to a western extension of the WPSH. At phase 1, the western edge of the 5880 line is located to the east of 130°E, and moves to the west of 130°E at phase 3. At phase 5, it extends to near

120°E. From phase 5 to 8, the area-mean Z'_{850} (ζ'_{850}) decreases (increases) gradually, resulting in the eastern retreat of the WPSH. The time series of area-mean Z'_{850} and ζ'_{850} in the key area from phase 1 to 8 are omitted.

Figure 9 shows the composite OLR' and 850-hPa wind anomaly during active WNP-QBWO events for eight phases. The QBWO active/suppressed convection center shows a northwestward propagation also vividly depicted in Fig. 9. In phase 8 and 1, the active convection center is located at the SCS, and meanwhile the suppressed convection center is located at the WNP (i.e., the diagonal area of phase 1 and 8 shown in Fig. 9). During phase 2 and 3, the active and suppressed centers propagates northwestward to East Asia and the diagonal area shown in Fig. 9 (Philippine Sea), respectively. In phase 4 and 5, the situation is opposite to the diagonal phase (phase 8 and 1 shown in Fig. 9), namely, the inactive convection center propagates to the SCS, and a new active convection center appears at the WNP. The situation in phase 6 and 7 is also opposite to the diagonal phase (phase 2 and 3), that is, the active and suppressed center is located at Philippine Sea and East Asia, respectively. As shown, the WPSH gradually moves westward from phase 1 to 5, and reaches the westernmost spot in phase 5. After that, the WPSH shows an eastern retreat from phase 6 to 8. It is the northwestward propagation of the WNP-QBWO that leads to the zonal oscillation of the WPSH. Once a suppressed convection center and an associated anticyclonic circulation propagates to the SCS, the WPSH shows a westward extension; once an active convection center and an associated cyclonic circulation reaches to the SCS, the WPSH shows an eastward retreat. Since the

WNP-QBWO state can be monitored and predicted by using the real-time index, the zonal location of the WPSH can also be monitored and predicted according to the WNP-QBWO state at an extended lead time.

As shown in Fig. 9, on the quasi-biweekly timescale when an anomalous anticyclone reaches the SCS-Philippine Sea (see phase 4), the WPSH extends westward, and the tropical southwesterly blows towards the Yangtze Basin, inducing positive rainfall anomaly (i.e., negative OLR anomaly) over there. In contrast, when an anomalous cyclone reaches the SCS-Philippine Sea (see phase 8), the WPSH retreats eastward, strong southwesterly blow mainly towards the SCS-Philippine Sea and the Yangtze Basin is dominated by a dry condition. Therefore, the QBWO of the WPSH's zonal shift is associated with a seesaw pattern of rainfall anomalies between the Yangtze Basin and the SCS-Philippine Sea which pattern is also revealed by Mao et al. (2010) and Guan et al. (2019). As for the air temperature anomaly related to the WPSH's zonal shift on the biweekly timescale, it is closely related to the rainfall anomaly, that is, more (less) rainfall in general corresponds to lower (higher) near-surface temperature (figure omitted). It is worth mentioning that on an interannual/interdecadal timescale the zonal oscillation of the WPSH can also affects the rainfall anomaly in the East Asian monsoon region. Generally speaking, the westward extension of the WPSH is associated with more rainfall in the East Asian monsoon region, since the flow at the northwestern edge of the WPSH transports a large amount of water vapor into this region (Lu, 2001; Huang et al., 2015). Through producing low cloudiness, clear skies, and warm advection, the westward expansion

of the WPSH also has an important role in summer extreme high temperature events over the East Asia summer monsoon region, including East China, South Korea, and Japan, on the interannual/interdecadal timescale (He and Gong, 2002; Meehl and Tebaldi, 2004; Ding et al., 2009; Yoon et al., 2018).

To sum up, the northwestward propagation of the WNP-QBWO leads to the zonal oscillation of the WPSH. To capture the leading signals of the QBWO mode in the WNP, an empirical orthogonal function (EOF) analysis is performed on the OLR' field in the domain of 0°–35°N, 110°–160°E (total 315 points in space) for summers from 1979 to 2013. The variance contributions of the first two modes (EOF1, EOF2) are 10.3% and 9.1%, respectively. They are statistically independent from higher modes based on the estimation of error range of eigenvalues proposed by North et al. (1982). The maximum/minimum time-lag correlation coefficient between the first two principal components (PC1, PC2) appears when PC1 leads/lags PC2 by 3 days (figure omitted). The significant lagged correlation indicates that EOF1 and EOF2 reflect a same propagating mode at different time phases. One can use PC1/PC2 for composite purpose to reveal the northwestward propagation feature of the WNP-QBWO, which is similar to that by using WNP-QBWOI. However, the reason why the WNP-QBWO moves northwestward is not very clear from now on. The northwestward propagation of the atmospheric WNP-QBWO was reported by a case study by Chen and Sui (2010). They mainly investigated the development and maintenance of the QBWO from energy (including eddy kinetic energy and eddy available potential energy) conversion perspective. Next, we will describe the possible mechanisms of the

northwestward propagation of the QBWO mode over the WNP. It is seen in Fig. 8 that a positive ζ'_{850} center is generally located to the northwest of a negative OLR' center. This positive vorticity anomaly at the top of the planetary boundary layer (PBL) induces a PBL convergence. The convergence leads a positive specific humidity anomaly (figure omitted), resulting in an increase of convection heating to the northwest of the convection anomaly center. Thus, the QBWO convection propagates northwestward.

The asymmetric structure with respect to the convection center can be vividly depicted by the meridional-vertical profile of the anomaly fields associated with the northward propagating 10–20-day OLR (Fig. 10). All fields shown in Fig. 10 are the average from day −7 to day 0 based on PC1, when the propagating convection originated from tropical area is generally located at the WNP. Day 0 is defined as when positive/negative OLR' center is located over 15°–20°N, 120°–130°E, where a negative center appears in EOF1.

The abscissa axis denotes meridional distance from the convection center (i.e., minimum OLR'), and the ordinate denotes pressure. It is shown that the maximum vertical velocity appears at the middle troposphere and is consistent with the convection center (Fig. 10a). The asymmetric vorticity (Fig. 10b) induces an asymmetric divergence (Fig. 10c) and specific humidity (Fig. 10d), that is, the positive vorticity anomaly ahead of the convection results in a northward shift of the PBL convergence through Ekman pumping, and then an increase of the moisture to the north of the convection center.

A vertical shear mechanism can interpret why the vorticity anomaly is located at the northwest of the convection anomaly center. In a 2.5-layer model (Wang and Li, 2003, 2004), the generation of the barotropic mode in the free atmosphere can only be realized via the vertical shear of the mean flow acting on the meridional gradient of the baroclinic divergence. The generation of the barotropic vorticity maybe further induces the development of the barotropic divergence in the free atmosphere. The prevailing easterly shear over the WNP region (figure omitted) can lead to the generation of the barotropic vorticity to the north of the convection. The detail process can be referred to Jiang et al. (2004). A moisture-convection feedback mechanism can interpret why the specific humidity anomaly appears to the northwest of the convection anomaly center. The observed summer mean flow over the WNP shows a prevailing northward component in the PBL (figure omitted). The moisture anomaly advection by this northward summer mean flow in the PBL together with the advection of the mean specific humidity by the perturbation vertical motion in the PBL is responsible for the asymmetry of the specific humidity with respect to the convection. The detail of this moisture-convection feedback process can also be referred to Jiang et al. (2004).

The above analysis suggests the internal dynamic process in the atmosphere is likely responsible for the northwestward propagation of the QBWO mode over the WNP. This internal atmosphere dynamics were previously used to explain the northward propagation of the intraseasonal oscillation in the south Asian monsoon region and SCS region (e.g., Jiang et al., 2004; Wang and Duan, 2015).

Ren et al. (2013) and Guan et al. (2019) reported that the local air-sea interaction in the WNP can cause the zonal shift of the WPSH on an intraseasonal timescale. They pointed out that a positive SST anomaly is generated beneath the western edge of the WPSH forced by a westward extension of the WPSH. The positive SST anomaly in turn has a negative feedback on the WPSH, which leads to an eastward retreat of the WPSH. We suppose that the tropical SST anomaly, through affecting the northwestward propagation of the QBWO mode over the WNP, also plays an important role in the zonal oscillation of the WPSH.

As shown in Fig. 11, a positive SST' anomaly (shading) in the WNP presents a northwestward propagation from phase 1 to 8. Of most interest is that the maximum/minimum SST' center leads the active/inactive convection center in the northwestward propagating journey, that is, the positive/negative SST' center is located to the northwest of the active/inactive convection center. This SST'-OLR' relationship can be depicted vividly by phase section of the SST' and OLR'. A spatial-phase evolution of SST' and OLR' along the line segment from 7.5°N, 145°E to 22.5°N, 117.5°E (red line in Fig. 11) is shown in Fig. 12. It is found that the active/inactive convection center lags the positive/negative SST' center for about 90-degree phase. A significant negative correlation (SST' leads Z'_{850}) suggests the impact of the SST' on the atmosphere. According to Lindzen and Nigam (1987), a positive SST anomaly may result in a boundary layer convergence via changing the boundary layer temperature and pressure. Thus, the positive SST' may lead to a convective instability (Wu, 2010) to the northwest of the negative OLR', resulting in

a northwestward shift of the QBWO convection.

A marked positive correlation (Z'_{850} leads SST′) indicates the effect of the atmosphere on the SST′. One possible process is the convection suppression related to the positive OLR′ to the northwest of the positive SST′ (see Fig. 12), in which a warming SST′ is induced through an increased downward short-wave radiation during the northward propagating journey of the OLR′. Another is the anomalous easterly, associated with the cyclonic anomaly to the northwest of the convection center (see vector in Fig. 11), opposes on the summer mean westerly, reducing the surface wind speed, and inducing a decrease of the upward latent heat flux from the ocean to atmosphere and then a warming SST′ to the northwest of the convection. Cao et al. (2017) reported that this cloud radiation effect and wind-evaporation effect on the quasi-biweekly scale are two important factors for the SCS-WNP SST′ northwestward propagation. We deem that the northwestward propagation of the WNP-QBWO arises from internal atmospheric dynamics as well as atmosphere-ocean interaction.

5. Conclusion and discussion

The main purpose of this study is to investigate the intraseasonal oscillation of the zonal shift of the WPSH during boreal summer and its possible mechanism. We first investigated the structure and evolution of the zonal oscillation of the WPSH at lower- and mid-troposphere on a quasi-biweekly timescale. Since the WPSH is most stable and strongest at the lower-troposphere and a maximum vorticity STD appears

in a key area (20°–30°N, 120°–140°E) over the western edge of the climatological WPSH, the lower-tropospheric vorticity (ζ_{850}) in this key area is selected to define an index to examine the main periodicity of the zonal shift of the WPSH. We revealed that the zonal movement of the WPSH exhibits a significantly 10–20-day oscillation. Based on a composite analysis we found that the Z' and ζ' exhibits an equivalent barotropic structure, and follows a quasi-geostrophic relationship well in the key area. With the quasi-biweekly variation of the geopotential height or vorticity in the key area, the WPSH shows a 10–20-day zonal oscillation at both mid- and lower-troposphere. The composite patterns indicate that the zonal shift of the WPSH is closely related to the northwestward propagation of the QBWO mode over the WNP. Thus, the relationship between the QBWO of the WPSH zonal shift and the northwestward-propagating QBWO over the WNP region, which was paid less attention in previous studies, is focused on in this study.

We propose a possible mechanism of the zonal shift of the WPSH on the quasi-biweekly time scale, in which the northwestward-propagating WNP-QBWO inducing the alternation of a positive and a negative height anomaly over the western edge of the climatological WPSH plays an essential role. Based on a real-time index of WNP-QBWO proposed recently, a WNP-QBWO cycle is divided into eight phases. A phase-composite patterns show that the convection anomaly propagates northwestward from the tropical WNP to East China. The associated vorticity or geopotential height also propagates northwestward. The QBWO of the WPSH zonal movement is caused by the gradual alternation of a positive and a negative

geopotential height anomaly originated from the tropical WNP. Once a positive (negative) QBWO geopotential height propagates from tropical WNP into the key area, it superimposes on the climatological WPSH and leads to a more western (eastern) edge of the WPSH than that of the climatological WPSH. During the northwestward-propagating journey of the QBWO over the WNP, the intensity of the geopotential height anomaly gradually changes, resulting in the zonal oscillation of the WPSH. Since the real-time WNP-QBWO index can be used for monitoring and predicting the WNP-QBWO's state, the influence of the WNP-QBWO on the zonal shift of the WPSH provide a monitoring and predicting method of the zonal shift of the WPSH at an extended rang by using the real-time index.

We pointed out that both the internal atmosphere dynamics and atmosphere-ocean interaction are responsible for the northwestward propagation of the QBWO mode over the WNP. A positive vorticity anomaly at the top of the PBL leads to an increase of the moisture during the northwestward journey. Both the positive vorticity and positive moisture anomaly is located to the northwest of the convection anomaly center, inducing the northwestward propagation of the QBWO convection. This vorticity-OLR relationship may be explained by the vertical shear mechanism proposed by Jiang et al. (2004). The local air-sea relationships on 10–20-day and 30–60-day time scales were compared by Ye and Wu (2015), but did not examine the physical mechanism of northwestward propagation of the QBWO mode. The SST' related to the QBWO convection also propagates northwestward over the WNP. A positive SST' is located to the northwest of the QBWO convection center.

The positive SST' leads the QBWO convection by an approximately 90-degree phase contributing to the northwestward propagation of the QBWO convection. Meanwhile, the atmosphere also contributes to the northwestward propagation of the SST' through cloud-radiation effect and wind-evaporation effect on the quasi-biweekly scale.

To sum up, the main conclusion of the current study is that there is a close relationship between the zonal shift of the WPSH and the northwestward-propagating QBWO over the WNP. In addition, we point out that both the internal atmospheric dynamics and the atmosphere-ocean interaction play a role in causing the northwestward propagation of the QBWO mode.

The large-scale mean circulation also has an important role in the propagation of the WNP-QBWO convection. As revealed by some previous studies, the mean state SST increases in the Pacific and shows an El Niño-like warming pattern in the equatorial Pacific under global warming (e.g., Xie et al., 2010; Ose and Arakawa, 2011). The enhanced surface evaporation induced by the mean SST warming leads to an increase in low-level water vapor, which is favorable to the increase in precipitation over the Pacific (Cui and Li, 2019). The convection therefore is more activity over the Pacific under global warming. We speculate that such a background change may lead to an enhanced WNP-QBWO intensity, which may give rise to an increase in the northwestward phase speed and a decrease in the periodicity of the WNP-QBWO mode. Therefore, the periodicity of the WPSH's zonal shift, which is caused by the northwestward propagation of the WNP-QBWO mode, may be

shortened but still within the quasi-biweekly timescale with global warming. However, the above speculation needs to be investigated in detail. One can use multiple CMIP5 (the Coupled Model Intercomparison Project, Phase 5) or CMIP6 (CMIP, phase 6) model datasets in historical runs and different scenario simulations to estimate the changes of the WPSH's zonal oscillation characteristics and the associated temperature and rainfall patterns under global warming.

It is worth noting that, besides being affected by the QBWO mode originated from tropical WNP in the mid-lower troposphere, the QBWO of the WPSH's zonal shift can also be influenced by the migration of the SAH in subtropical region in the upper troposphere (Guan et al., 2018). On the other hand, the anomalous diabatic heating, induced by the opposite movement of the QBWO of the WPSH, also plays a role in the zonal shift of the SAH (Ren et al., 2015). Therefore, there is an interaction between the zonal movement of the SAH and the WPSH. The mid-high-latitude wave train across Eurasia impacts the zonal shift of the SAH on the biweekly timescale. Since the wave train propagates southeastward, a geopotential height anomaly from western flank of the Tibetan Plateau (TP) to the east of TP contributes to the zonal movement of the SAH (Ren et al., 2015). In addition, the circulation over the TP also possesses remarkable QBWO disturbance, and the aforementioned mid-high-latitude wave train plays an important role in the TP-QBWO (Yang and Li, 2017; Wang et al., 2019). The major body of the SAH is located over the Tibetan Plateau (TP) and its neighboring area. Since the TP-QBWO and the QBWO movement of the SAH can be affected by the same wave train, there should be some relationship between them.

Given the relation of the SAH's QBWO zonal shift to the TP-QBWO and to the WPSH's QBWO zonal shift, there may have a connection between the QBWO of the SAH's zonal shift and the TP-QBWO, which needs further study.

The intraseasonal signals from upstream or mid-high latitudes may also influence the zonal movement of the WPSH, when the signals propagate eastward/southeastward to the western Pacific. It seems that the QBWO-induced zonal shift of the WPSH is accompanied by a meridional shift (see Fig. 8 and Fig. 10), that is, a westward extension is along with a southward shift, while an eastward retreat is accompanied by a northward movement. This co-movement of zonal and meridional oscillation may be one nature of the WPSH, which requires a further study in the future. It is displayed in Fig. 1 and Fig. 3 that the summer-mean relative vorticity and geopotential height shows a northeast-southwest tilt to some extent. However, the relationship between the northeast-southwest tilt and the northeastward/southwestward shift of the WPSH shift is unknow and needs a further investigation.

Acknowledgements. This work was supported by the National Key R&D Program of China (Grant No. 2018YFC1505803, 2018YFC1505602), the Natural Science Foundation of Jiangsu Higher Education Institutions of China (Grant No. 18KJB170015), the National Natural Science Foundation of China (Grant No. 41975048), and the Startup Foundation for Introducing Talent of NUIST (2018R027).

References

Cao X, Wu RG, Chen SF. 2017. Contrast of 10–20-day and 30–60-day intraseasonal SST propagation during summer and winter over the South China Sea and western North Pacific. Clim. Dyn. 48:1233–1248.

Chen GH, Sui C-H. 2010. Characteristics and origin of quasi-biweekly oscillation over the western North Pacific during boreal summer. J. Geophy. Res. Atmos. 115. doi:10.1029/2009JD013389.

Chen Y, Zhai P. 2016. Mechanisms for concurrent low-latitued circulation anomalies responsible for persistent extreme precipitation in the Yangtze River Valley. Clim. Dyn. 47:989–1006.

Cui J, and Li T. 2019. Changes of MJO propagation characteristics under global warming. Clim. Dyn. 53:5311-5327.

Dee D, Uppala S, Simmons A et al 2011. ERA-interim reanalysis: configuration and performance of the data assimilation system. Q. J. R. Meteorol. Soc. 137:553–597.

Ding T, Qian W, Yan Z. 2009. Changes in hot days and heat waves in China during 1961–2007. Int. J. Climatol. 30:1452–1462.

Duchon CE. 1979. Lanczos filtering in one and two dimensions. J. Appl. Meteor. 18:1016–1022.

Gong DY, Ho CH. 2002. Shift in the summer rainfall over the Yangtze River valley in the late 1970s. Geophys. Res. Lett. 29, 1436, doi:10.1029/2001GL014523.

Guan WN, Hu HB, Ren XJ, et al. 2019. Subseasonal zonal variability of the western

Pacific subtropical high in summer: climate impacts and underlying mechanisms. Clim. Dyn. 53:3325–3344.

Guan W, Ren X, Shang W, et al. 2018. Subseasonal zonal oscillation of the western Pacific subtropical high during early summer. J. Meteor. Res. 32:768–780

Ho CH, Baik JJ, Kim JH, Gong DY, and Sui CH. 2004. Interdecadal changes in summertime typhoon tracks. J. Clim. 17:1767–1776.

Huang Y, Wang H, Fan K, Gao Y. 2015. The western Pacific subtropical high after the 1970s: westward or eastward shift? Clim. Dyn. 44 2035–2047.

Jia X, Yang S. 2013. Impact of the quasi-biweekly oscillation over the western North Pacific on East Asian subtropical monsoon during early summer. J. Geophys. Res. Atmos. 118:4421–4434.

Jiang X, Li T, Wang B. 2004. Structures and mechanisms of the northward propagating boreal summer intraseasonal oscillation. J. Clim. 17:1022–1039.

Kanamitsu M, Ebisuzaki W, Woollen J, Yang SK, Hnilo J, Fiorino M, Potter G. 2002. NCEP-DOE AMIP-II reanalysis (r-2). Bull. Am. Meteorol. Soc. 83:1631–1643.

Lau KH, Lau NC. 1990. Observed structure and propagation characteristics of tropical summertime synoptic scale disturbances. Mon. Wea. Rev. 118:1888–1913.

Lau KM, Li MT. 1984. The monsoon over East Asia and its global association-A survey. Bull. Amer. Meteor. Soc. 65:116–125.

Lau KM, Weng H. 2002. Recurrent teleconnection patterns linking summertime precipitation variability over East Asia and North America. J. Meteorol. Soc. Japan. 80:1309–1324.

Liebmann B, Smith CA. 1996. Description of a complete (interpolated) outgoing longwave radiation dataset. Bull. Am. Meteorol. Soc. 77:1275–1277.

Lindzen RS, Nigam S. 1987. On the role of sea surface temperature gradients in forcing low-level winds and convergence in the tropics. J. Atmos. Sci. 44:2418–2436.

Liu H, Zhang DL, Wang B. 2008. Daily to submonthly weather and climate characteristics of the summer 1998 extreme rainfall over the Yangtze River basin. J. Geophys. Res. 113, D22101, doi:10.1029/2008JD010072.

Lu R. 2001. Interannual variability of the summertime North Pacific subtropical high and its relation to atmospheric convection over the warm pool. J. Meteor. Soc. Japan 79:771–783.

Lu R, Li Y, Ryu CS. 2008. Relationship between the zonal displacement of the western pacific subtropical high and the dominant modes of low-tropospheric circulation in summer. Prog. Nat. Sci. 18:161–165.

Mao J, Sun Z, Wu G. 2010. 20–50-day oscillation of summer Yangtze rainfall in response to intraseasonal variations in the subtropical high over the western North Pacific and South China Sea. Clim. Dyn. 34:747–761.

Matsumura S, Sugimoto S, Sato T. 2015. Recent intensification of the western Pacific subtropical high associated with the East Asian summer monsoon. J. Clim. 28:2873–2883.

Meehl GA, Tebaldi C. 2004. More intense, more frequent, and longer lasting heat waves in the 21st century. Science 305:994–997.

North GR, Bell TL, Cahalan RF, et al. 1982, Sampling errors in the estimation of empirical orthogonal functions. Mon. Wea. Rev. 110:699–706.

Ose T, Arakawa O. 2011. Uncertainty of future precipitation change due to global warming associated with sea surface temperature change in the tropical Pacific. J. Meteorol. Soc. Japan 89:539–552.

Qian Y, Hsu PC, Kikuchi K. New real-time indices for the quasi-biweekly oscillation over the Asian summer monsoon region. Clim. Dyn. doi: 10.1007/s00382-019-04644-0.

Ren X, Yang D, Yang X. 2015. Characteristics and mechanisms of the subseasonal eastward extension of the South Asian High. J. Clim. 28:6799–6822.

Ren X, Yang X, Sun X. 2013. Zonal oscillation of western Pacific subtropical high and subseasonal SST variations during Yangtze persistent heavy rainfall events. J. Clim. 26:8929–8946.

Sui CH, Chung PH, Li T. 2007. Interannual and interdecadal variability of the summertime western North Pacific subtropical high. Geophys. Res. Lett. 34, L11701, doiL10.1029/2006GL029204.

Wang B, Li T. 1993. A simple tropical atmospheric model of relevance to short-term climate variation. J. Atmos. Sci. 50:260–284.

Wang B, Li T. 1994. Convective interaction with boundary-layer dynamics in the development of a tropical intraseasonal system. J. Atmos. Sci. 51:1386–1400.

Wang B, Xiang B, Lee JY. 2013. Subtropical High predictability establishes a promising way for monsoon and tropical storm predictions. Proceedings of the

National Academy of Sciences, 110:2718–2722.

Wang HJ, Chen HP. 2012. Climate control for Southeastern China moisture and precipitation: Indian or East Asian Monsoon? J. Geophys. Res. 117. doi:10.1029/2012JD017734.

Wang M, Duan A. 2015. Quasi-biweekly oscillation over the Tibetan Plateau and its link with Asian summer monsoon. J. Clim. 28:4921–4940.

Wang M, Wang J, Duan A, et al. 2019. Quasi-biweekly impact of the atmospheric heat source over the Tibetan Plateau on summer rainfall in Eastern China. Clim. Dyn. 53:4489–4504.

Wei W, Zhang R, Wen M, Yang S, et al. 2019. Dynamic effect of the South Asian high on the interannual zonal extension of the western North Pacific subtropical high. Int. J. Climatol. 39: 5367–5379.

Wen M, Yang S, Higgins W, Zhang R. 2011. Characteristics of the dominant modes of atmospheric quasi-biweekly oscillation over tropical-subtropical Americas. J Clim. 24:3956–3970.

Wu B, T Zhou. 2008. Oceanic origin of the interannual and interdecadal variability of the summertime western Pacific subtropical high. Geophys. Res. Lett. 35, L13701, doi:10.1029/2008GL034584.

Wu R. 2010. Subseasonal variability during the South China Sea summer monsoon onset. Clim. Dyn. 34:629–642.

Xie SP, Deser C, Vecchi GA, et al. 2010. Global warming pattern formation: sea surface temperature and rainfall. J. Clim. 23:966–986.

Yanai M, Esbensen S, Chu JH. 1973. Determination of bulk properties of tropical cloud clusters from large-scale heat and moisture budgets. J. Atmos. Sci. 30:611–627.

Yang J, Wang B, Wang B, et al. 2010. Biweekly and 21-30-day variations of the subtropical summer monsoon rainfall over the lower reach of the Yangtze River basin. J. Clim. 23:1146–1159.

Yang S, Li T. 2016. Zonal shift of the South Asian High on the subseasonal time-scale and its relation to the summer rainfall anomaly in China. Q. J. R. Meteorol. Soc. 142:2324–2335.

Yang S, Li T. 2017a. Causes of intraseasonal diabatic heating variability over and near the Tibetan Plateau in boreal summer. Clim. Dyn. 49:2385–2406.

Yang S, Li T. 2017b. The role of intraseasonal variability at mid-high latitudes in regulating Pacific blockings during boreal winter. Int. J. Climatol. 37(s1):1248–1256.

Ye KH, Wu RG. 2015. Contrast of local air–sea relationships between 10–20-day and 30–60-day intraseasonal oscillations during May–September over the South China Sea and western North Pacific. Clim. Dyn. 45:3441–3459.

Yoon D, Cha DH, Lee G, et al. 2018. Impacts of synoptic and local factors on heat wave events over southeastern region of Korea in 2015. J. Geophy. Res. Atmos. 123:12081–12096.

List of Figure Captions

Fig. 1 (a) Day-to-day standard deviation (contour; normalized by the zonal mean) of 36-summer (1979–2014; JJA) non-filtered ζ_{850} anomaly (with the mean and first four harmonics of annual cycle removed) and summer-mean ζ_{850} (shading; 10^{-6} s^{-1}); the box (20°–30°N, 120°–140°E) indicates the area selected to define the relative vorticity index (RVI) of WPSH. (b), (c), (d) As in (a), but for ζ_{500}, Z_{850} and Z_{500} (unit of shading: gpm), respectively. Dashed isoline in (c) and (d) respectively represents 1520-line and 5880-line

Fig. 2 Composite (a)–(b) ζ_{850}, (c)–(d) Z_{850} and (e)–(f) Z_{500} during the RVI (a), (c), (e) less than its –1.0 standard deviation (-1.0σ) and (b), (d), (f) greater than its $+1.0\sigma$. Unit for ζ is 10^{-6} s^{-1}, and unit for Z is gpm. 1520 and 5880 gpm contours are highlighted in blue

Fig. 3 (a) Power spectral analysis of the RVI (with the mean and first four harmonics of annual cycle removed). Red solid curve is power spectrum; green solid line is red noise spectrum, dashed line denotes the 0.05 significance level. (b) Day-to-day standard deviation (contour; 10^{-6} s^{-1}) of the 10–20-day filtered ζ_{850}; shadings as in Fig. 1a. (c) As in (b), but for non-filtered ζ_{850} anomaly

Fig. 4 (a) Composite 10–20-day filtered geopotential height Z'_{850} (shadings) from day 0 to +6; doted areas exceed the 0.05 significance level. Solid contours are Z_{850} (interval: 20 gpm; 1520 gpm is highlighted in red) during eastward withdrawal events; red arrows indicate the zonal shift of the westernmost point of the ridge line. Composite is defined as eastward withdrawal event minus

westward extension event. (b) As in (a), but for 500 hPa; 5880 gpm is highlighted in blue

Fig. 5 (a) Composite ζ'_{850} (shadings; 10^{-6} s^{-1}; all shadings exceed the 0.05 significance level) and OLR' (contour; interval: 3.0 W m^{-2}; zero contours omitted; the dotted grids exceed the 0.05 significance level) from day –6 to 0; (b) As in (a), but shadings for $<Q_1>'$ (W m^{-2})

Fig. 6 Phase propagation vectors (arrows; m s^{-1}; see scale at the upper left corner) and the temporal coherence (shading; see scale bar) of ζ'_{850}. Shadings indicating the phase velocity surpassing 0.05 significance level

Fig. 7 WNP-QBWO phase space diagram based on WNP-QBWOI1 and WNP-QBWOI2. The first number in each phase denotes active WNP-QBWO events (i.e., amplitude >1.0); the number in brackets means the average amplitude of the active events in each phase

Fig. 8 Composite OLR' (shadings; W m^{-2}) and ζ'_{850} (contour; 10^{-6} s^{-1}; zero contour omitted; all contours surpass the 0.05 significance level) for eight phases of the WNP-QBWO life cycle during active WNP-QBWO events. Only shadings surpass 0.05 significance level are shown. Thick lines indicate the associated 5880 isoline. The composite sample in each phase is shown in Fig. 7. For example, the composite sample in phase 1 is 232

Fig. 9 As in Fig. 8, but the vectors for 850-hPa wind anomaly (m s^{-1}); Only vectors surpass 0.05 significance level are shown

Fig. 10 Meridional-vertical distribution of 10–20-day filtered (a) vertical velocity

(interval: 3.0×10^{-3} Pa s^{-1}), (b) vorticity (interval: 6.0×10^{-7} s^{-1}), (c) divergence (interval: 1.0×10^{-7} s^{-1}), (d) specific humidity (interval: 5.0×10^{-5} kg kg^{-1}) associated with the northward propagating 10–20-day OLR. Shadings exceed the 0.05 significance level. Positive/negative value in x-axis means the meridional (°lat) distance to the north/south of the convection center. For instance, if convection center is at (0°lon, 0°lat), then 3 means location at (0°lon, 3°lat). Y-axis is pressure (hPa). All composite fields here are the average from day −7 to day 0 based on PC1

Fig. 11 As in Fig. 8, but shading for SST' (K), vector for 10m-wind (m s^{-1}), and blue contours for OLR' (contour interval: 4 W m^{-2}; zero contour omitted; all contours surpass the 0.05 significance level), dotted area indicates SST' surpassing the 0.05 significance level

Fig. 12 Hovmöller plots of composite fields along line 7.5°N, 145°E–22.5°N, 117.5°E (red line in Fig. 11). Contour is OLR' (interval: 2 W m^{-2}); shading is SST' (K)

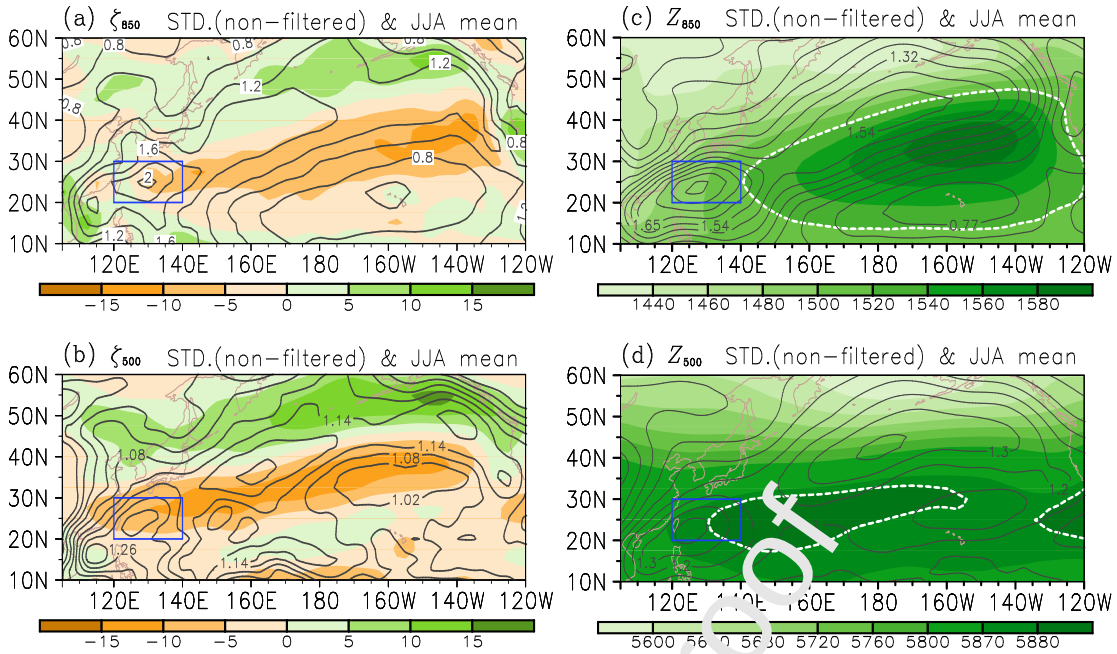

Fig. 1 (a) Day-to-day standard deviation (colour; normalized by the zonal mean) of 36-summer (1979–2014; JJA) non-filtered ζ_{850} anomaly (with the mean and first four harmonics of annual cycle removed) and summer-mean ζ_{850} (shading; 10^{-6} s^{-1}); the box (20°–30°N, 120°–140°E) indicates the area selected to define the relative vorticity index (RVI) of WNPSH. (b), (c), (d) As in (a), but for ζ_{500}, Z_{850} and Z_{500} (unit of shading: gpm), respectively. Dashed isoline in (c) and (d) respectively represents 1520-line and 5880-line

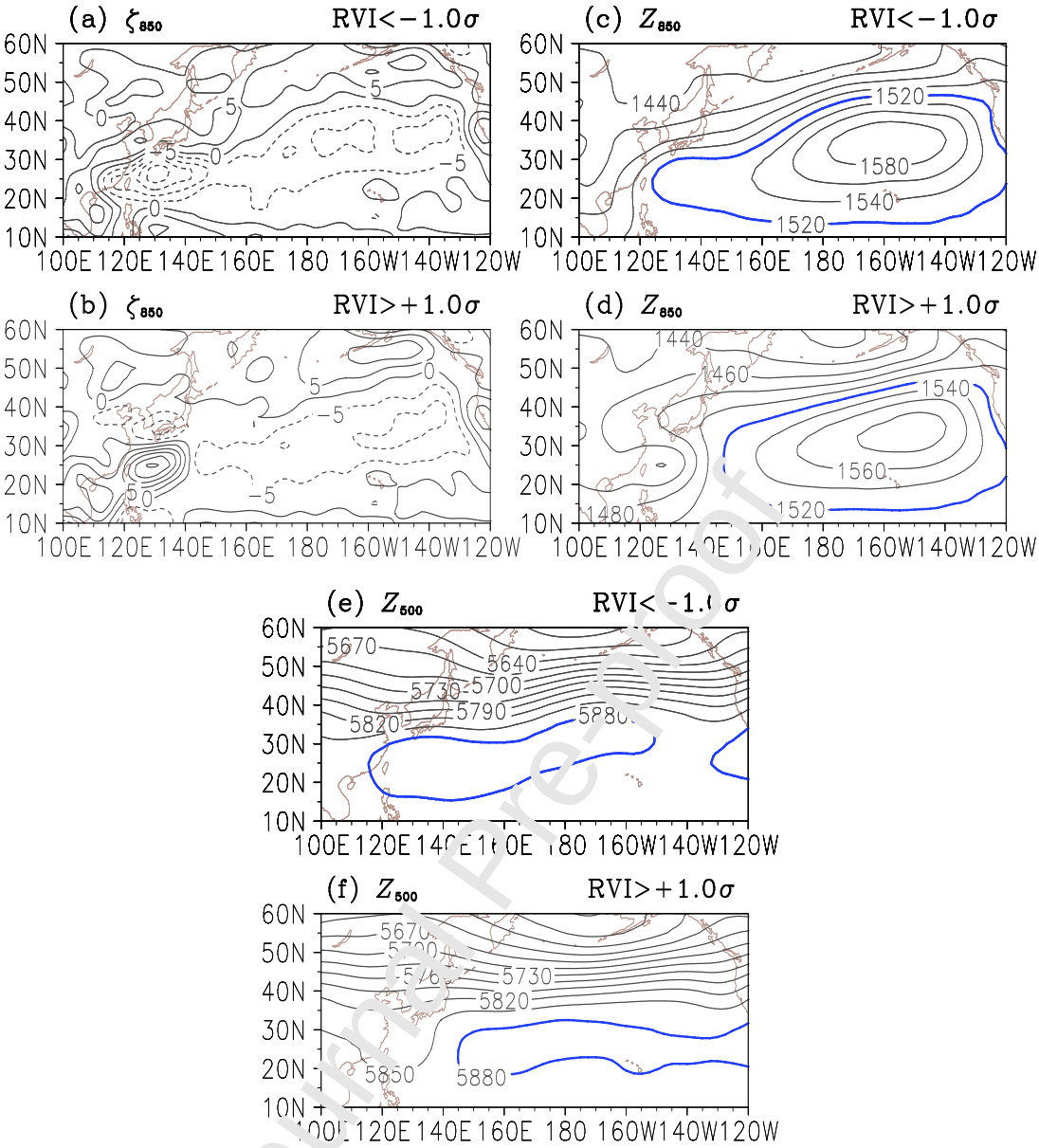

Fig. 2 Composite (a)–(b) ζ_{850}, (c)–(d) Z_{850} and (e)–(f) Z_{500} during the RVI (a), (c), (e) less than its –1.0 standard deviation (–1.0σ) and (b), (d), (f) greater than its +1.0σ. Unit for ζ is 10^{-6} s^{-1}, and unit for Z is gpm. 1520 and 5880 gpm contours are highlighted in blue

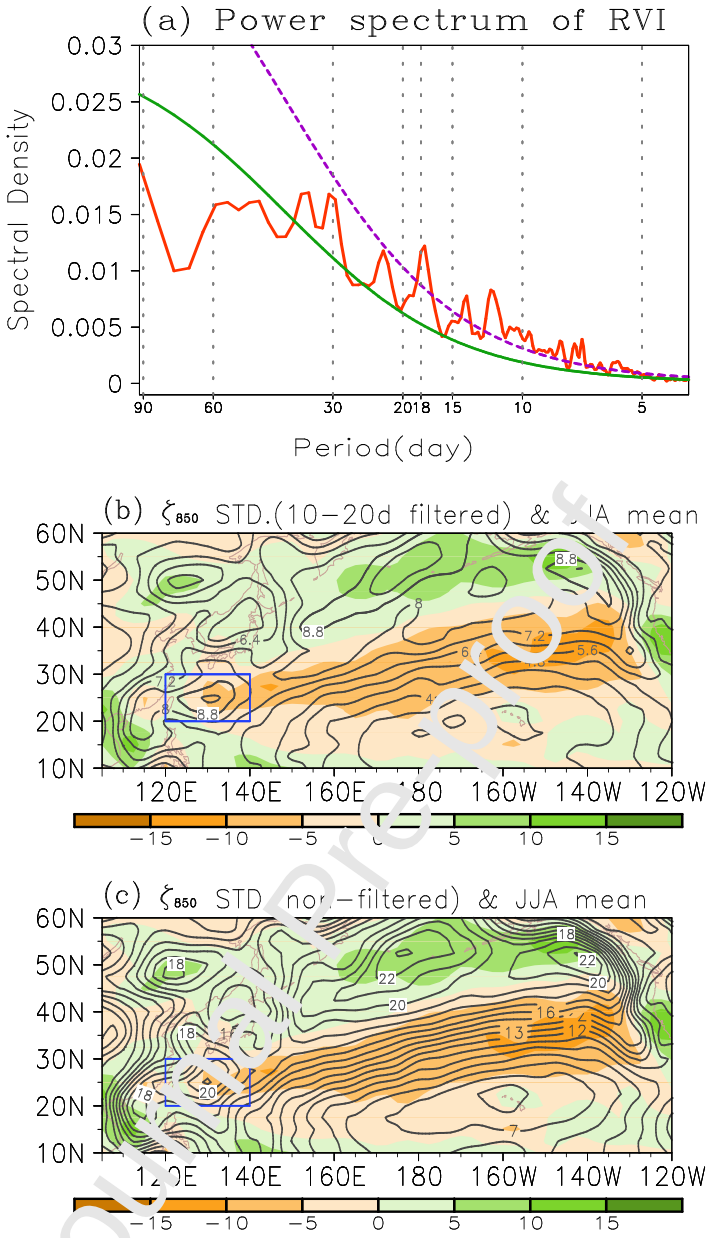

Fig. 3 (a) Power spectral analysis of the RVI (with the mean and first four harmonics of annual cycle removed). Red solid curve is power spectrum; green solid line is red noise spectrum; dashed line denotes the 0.05 significance level. (b) Day-to-day standard deviation (contour; 10^{-6} s^{-1}) of the 10–20-day filtered ζ_{850}; shadings as in Fig. 1a. (c) As in (b), but for non-filtered ζ_{850} anomaly

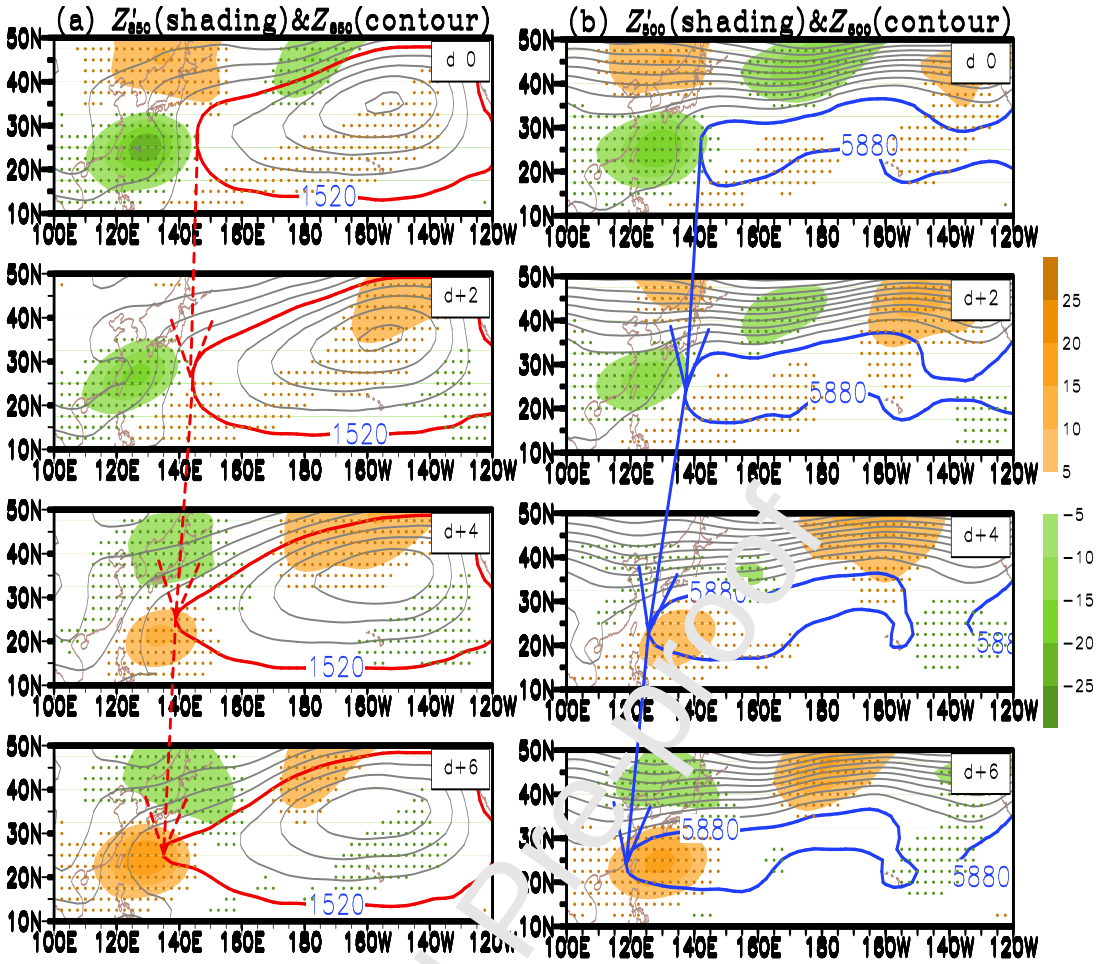

Fig. 4 (a) Composite 10–20-day filtered geopotential height Z'_{850} (shadings) from day 0 to +6; doted areas exceed the 0.05 significance level. Solid contours are Z_{850} (interval: 20 gpm; 1520 gpm is highlighted in red) during eastward withdrawal events; red arrows indicate the zonal shift of the westernmost point of the ridge line. Composite is defined as eastward withdrawal event minus westward extension event. (b) As in (a), but for 500 hPa; 5880 gpm is highlighted in blue

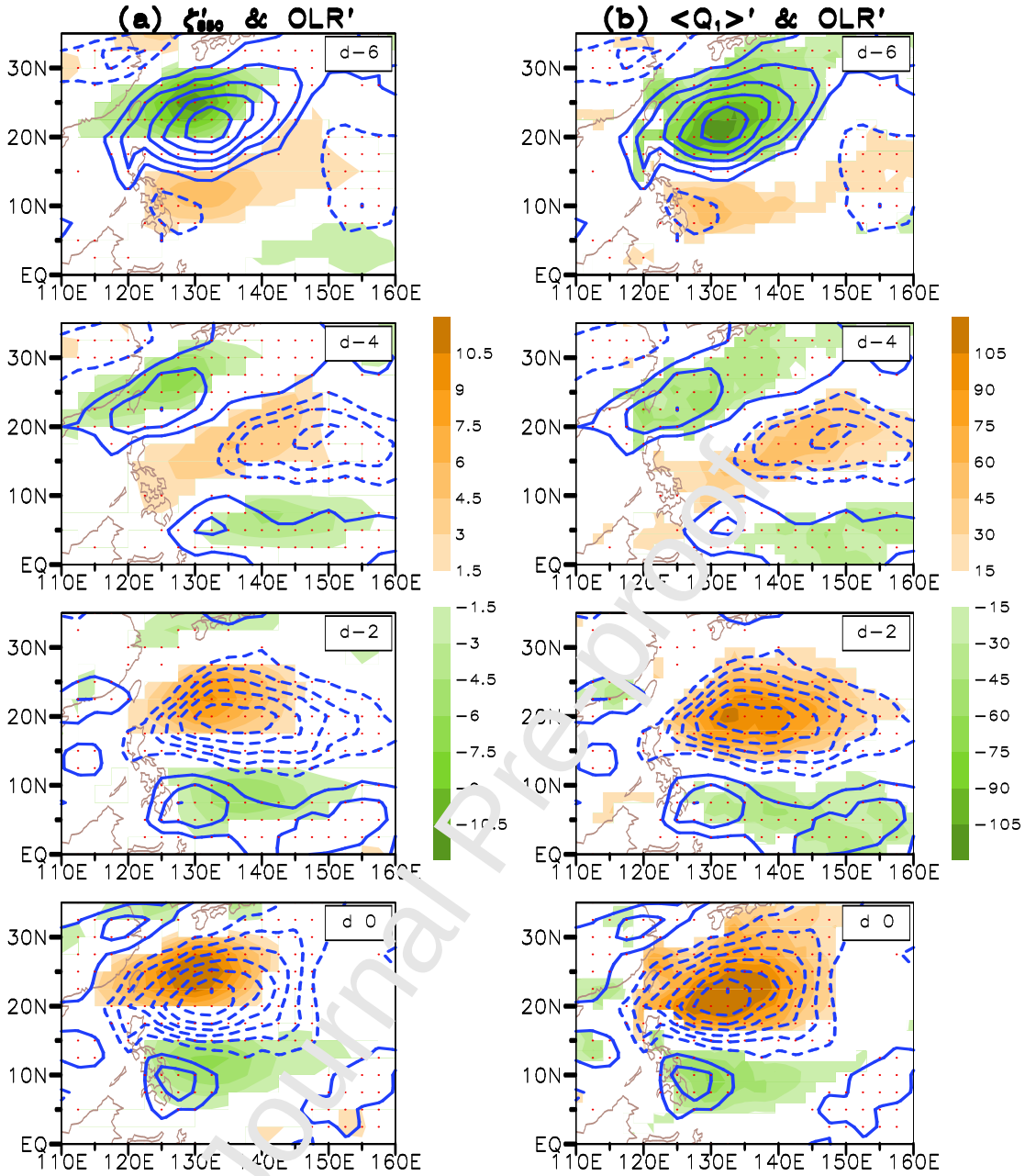

Fig. 5 (a) Composite ζ'_{850} (shadings; 10^{-6} s^{-1}; all shadings exceed the 0.05 significance level) and OLR' (contour; interval: 3.0 W m^{-2}; zero contours omitted; the dotted grids exceed the 0.05 significance level) from day –6 to 0; (b) As in (a), but shadings for $<Q_1>'$ (W m^{-2})

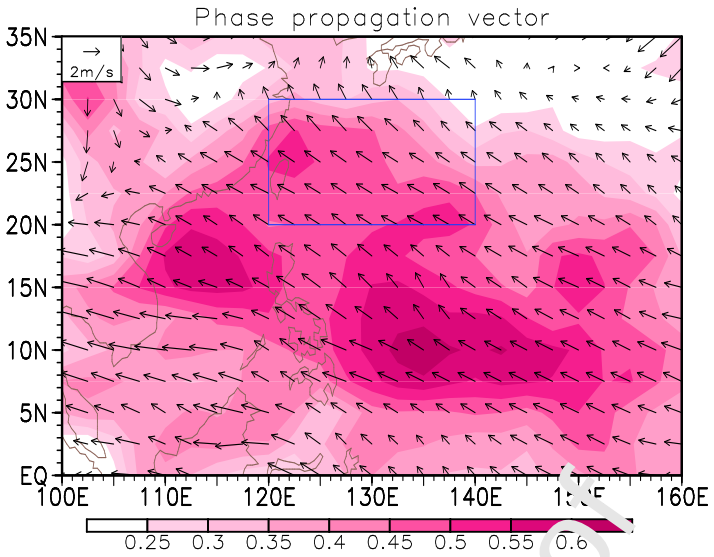

Fig. 6 Phase propagation vectors (arrows; m s^{-1}; see scale at the upper left corner) and the temporal coherence (shading; see scale bar) of ζ'_{850}. Shadings indicating the phase velocity surpassing 0.05 significance level

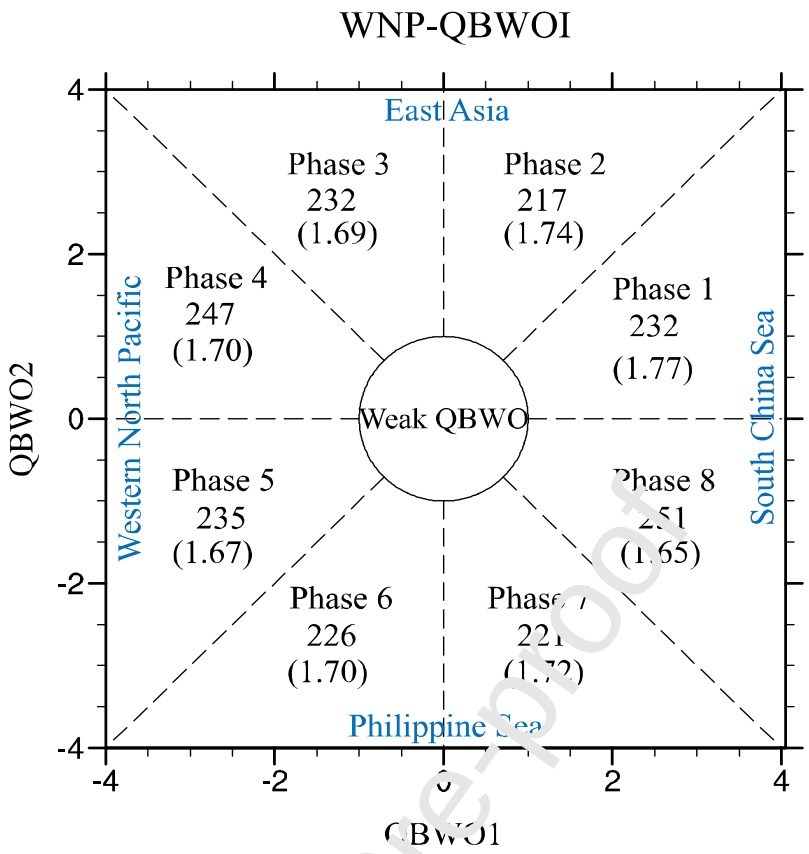

Fig. 7 WNP-QBWO phase space diagram based on WNP-QBWOI1 and WNP-QBWOI2. The first number in each phase denotes active WNP-QBWO events (i.e., amplitude >1.0); the number in brackets means the average amplitude of the active events in each phase

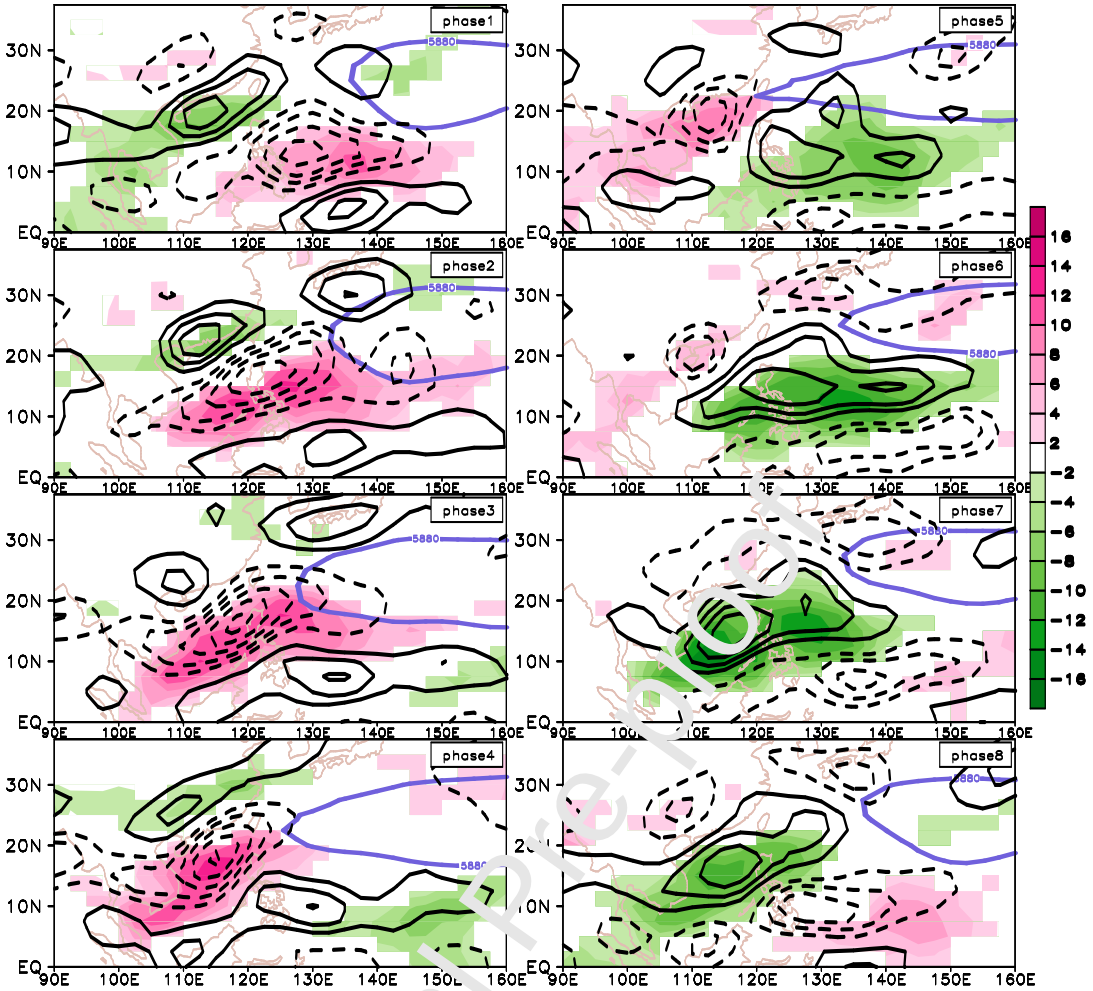

Fig. 8 Composite OLR' (shadings; W m^{-2}) and ζ'_{850} (contour; 10^{-6} s^{-1}; zero contour omitted; all contours surpass the 0.05 significance level) for eight phases of the WNP-QBWO life cycle during active WNP-QBWO events. Only shadings surpass 0.05 significance level are shown. Thick lines indicate the associated 5880 isoline. The composite sample in each phase is shown in Fig. 7. For example, the composite sample in phase 1 is 232

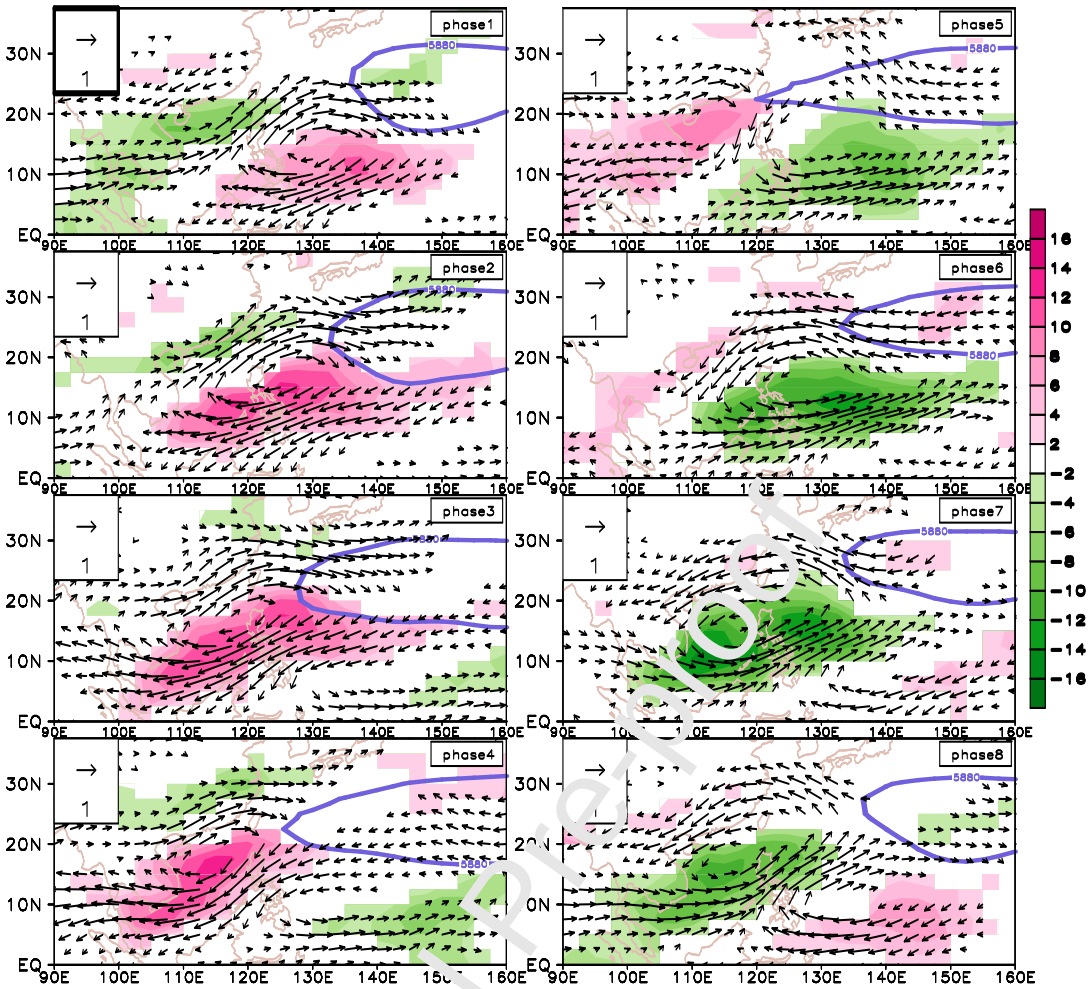

Fig. 9 As in Fig. 8, but the vectors for 850-hPa wind anomaly (m s^{-1}); Only vectors surpass 0.05 significance level are shown

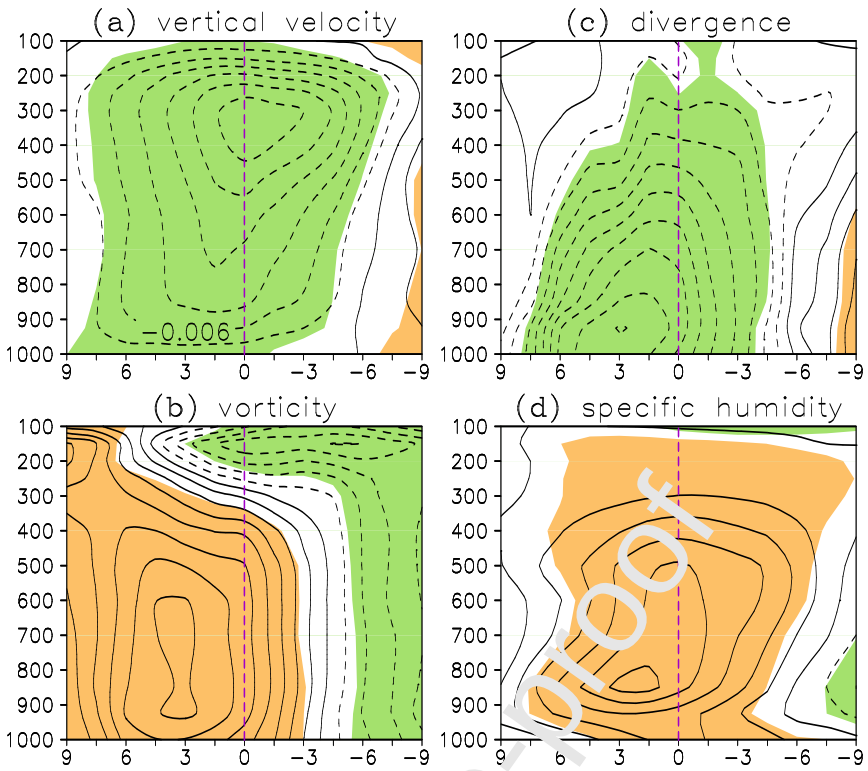

Fig. 10 Meridional-vertical distribution of 10–20-day filtered (a) vertical velocity (interval: 3.0×10^{-3} Pa s^{-1}), (b) vorticity (interval: 6.0×10^{-7} s^{-1}), (c) divergence (interval: 1.0×10^{-7} s^{-1}), (d) specific humidity (interval: 5.0×10^{-5} kg kg^{-1}) associated with the northward propagating 10–20-day OLR. Shadings exceed the 0.05 significance level. Positive/negative value in x-axis means the meridional (°lat) distance to the north/south of the convection center. For instance, if convection center is at (0°lon, 0°lat), then 3 means location at (0°lon, 3°lat). Y-axis is pressure (hPa). All composite fields here are the average from day −7 to day 0 based on PC1

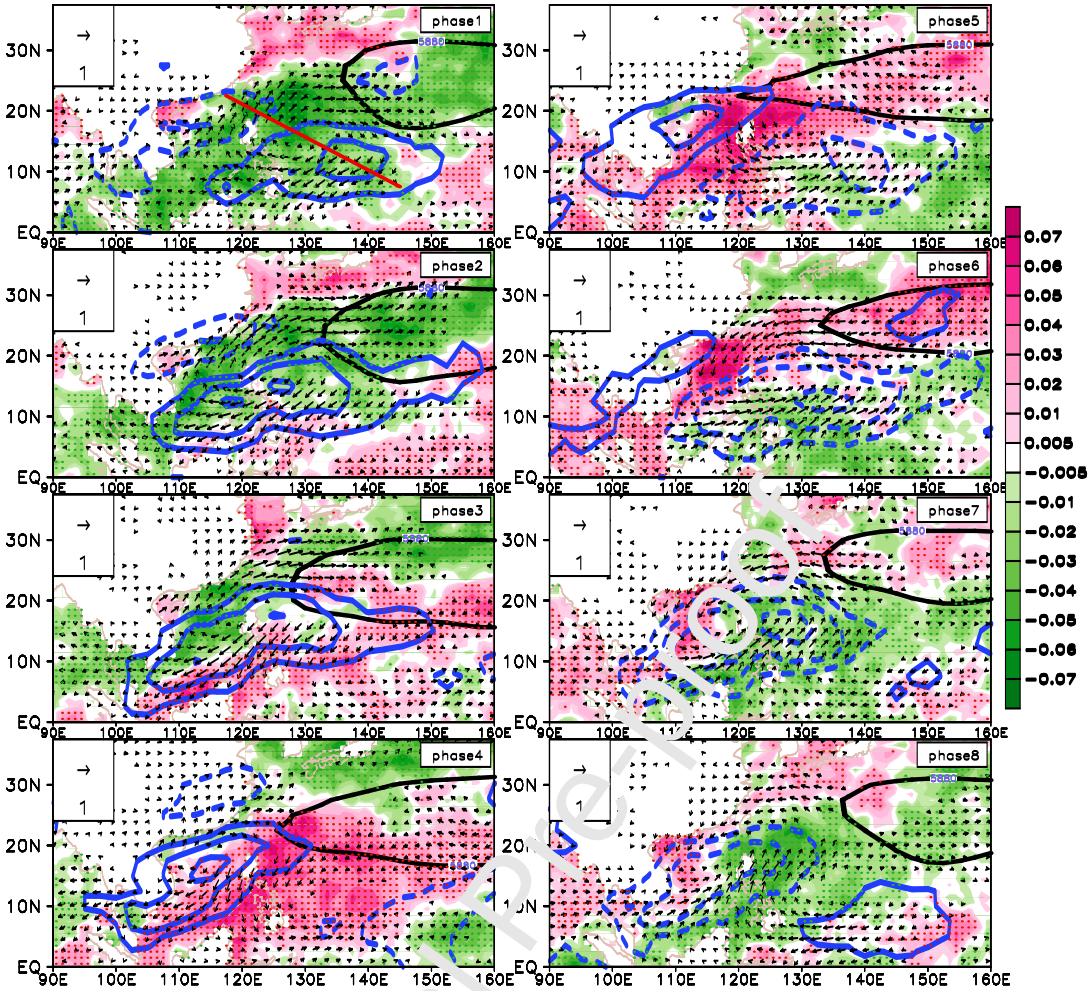

Fig. 11 As in Fig. 8, but shading for SST' (K), vector for 10m-wind (m s^{-1}), and blue contours for OLR' (contour interval: 4 W m^{-2}; zero contour omitted; all contours surpass the 0.05 significance level); doted area indicates SST' surpassing the 0.05 significance level

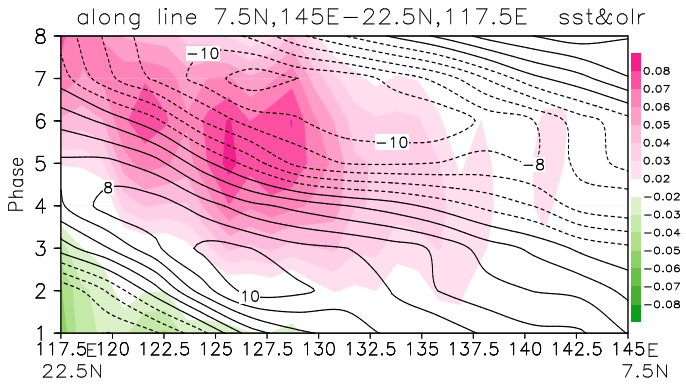

Fig. 12 Hovmöller plots of composite fields along line 7.5°N, 145°E–22.5°N, 117.5°E (red line in Fig. 11). Contour is OLR' (interval: 2 W m^{-2}), shading is SST' (K)

Shuangyan Yang: methodology, software, validation, formal analysis, investigation, resources, data curation, writing-original draft preparation, writing-review and editing, visualization, supervision, funding acquisition

Tim Li: Conceptualization, formal analysis, resources, writing-review and editing, supervision, project administration

Declaration of interests

☒ The authors declare that they have no known competing financial interests or personal relationships that could have appeared to influence the work reported in this paper.

☐The authors declare the following financial interests/personal relationships which may be considered as potential competing interests:

Highlights

- Zonal shift of WPSH exhibits a significantly 10–20-day oscillation
- Northwestward propagating WNP-QBWO causes WPSH zonal shift
- Alternation of a positive/negative height anomaly leads to WPSH zonal shift
- Internal atmospheric dynamics is responsible for WNP-QBWO propagation
- Atmosphere-ocean interaction is also responsible for WNP-QBWO propagation